ACS Synthetic Biology

pubs.acs.org/synthbio

Research Article

Optimization of RNA Pepper Sensors for the Detection of Arbitrary RNA Targets

Anli A. Tang, Anna Afasizheva, Clara T. Cano, Kathrin Plath, Douglas Black, and Elisa Franco*

Cite This: *ACS Synth. Biol.* 2024, 13, 498−508

Read Online

ACCESS | Metrics & More | Article Recommendations | Supporting Information

ABSTRACT: The development of fluorescent light-up RNA aptamers (FLAPs) has paved the way for the creation of sensors to track RNA in live cells. A major challenge with FLAP sensors is their brightness and limited signal-to-background ratio both *in vivo* and *in vitro*. To address this, we develop sensors using the Pepper aptamer, which exhibits superior brightness and photostability when compared to other FLAPs. The sensors are designed to fold into a low fluorescence conformation and to switch to a high fluorescence conformation through toehold or loop-mediated interactions with their RNA target. Our sensors detect RNA targets as short as 20 nucleotides in length with a wide dynamic range over 300-fold *in vitro*, and we describe strategies for optimizing the sensor's performance for any given RNA target. To demonstrate the versatility of our design approach, we generated Pepper sensors for a range of specific, biologically relevant RNA sequences. Our design and optimization strategies are portable to other FLAPs and offer a promising foundation for future development of RNA sensors with high specificity and sensitivity for detecting RNA biomarkers with multiple applications.

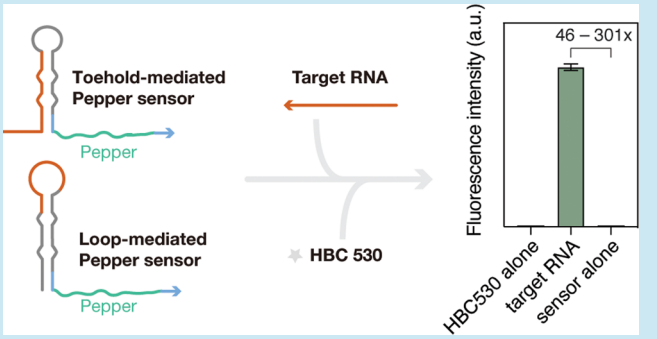

KEYWORDS: *fluorescent light-up aptamers, RNA sensors, toehold switches, loop switches*

1. INTRODUCTION

Fluorogenic RNA aptamers have emerged as powerful tools for real-time monitoring of RNA expression, localization, and dynamics in living cells. These RNA molecules, also known as fluorescent light-up aptamers (FLAPs), are selected to bind to fluorophores and undergo conformational changes that lead to fluorescence enhancement.[1] A multitude of FLAPs and cognate fluorophores have been demonstrated to work *in vitro* and within living cells: examples include aptamers known as Malachite Green,[2,3] GFP-mimics Spinach, Broccoli, and Corn,[4−7] Mango I−IV,[8,9] and Pepper.[10]

Recent advances in nucleic acid nanotechnology have made it possible to demonstrate FLAPs working as sensors that fluoresce specifically upon hybridization to the intended RNA target.[11,12] These target-responsive FLAP-based RNA sensors are genetically encoded but do not require any modifications to the RNAs of interest.[13] FLAP sensors simply need to be transcribed and hybridized to their RNA target, thereby activating their fluorogenic function (sensor ON). To be effective to detect and track RNA molecules in live-cell imaging, FLAP sensors should exhibit a low background fluorescence in the absence of the target (sensor OFF). A simple strategy to achieve this is to split RNA FLAPs in two nonfluorescent domains, whose assembly is seeded by the target nucleic acid.[11,12,14−16] Researchers have successfully demonstrated the recognition of endogenous mRNA in mammalian cells and RNA imaging in *Escherichia coli* using this approach.[11,12,16] Another approach is that of designing the FLAP so that it fluoresces only upon binding to its RNA target and undergoing a conformational change while otherwise remaining in the OFF state. This approach has the advantage of requiring transcription of a unimolecular sensor component with high specificity for its target; further, the FLAP secondary structure is programmable *via* sequence design,[17] and its conformational changes can be optimized to maximize the ON/OFF ratio.[18−26] Although existing FLAP-based RNA sensors (Table S1) enable the noninvasive visualization of endogenous mRNAs in living cells, imaging targets at low copy number remains a challenge because it requires both the brightness of the ON FLAP sensor and low OFF signal.

A promising candidate to build RNA sensors for low abundance targets is "Pepper" (Figure 1A1), a 43-nucleotide FLAP that was shown to exhibit higher brightness and photostability when compared to other established fluorogenic aptamers including Broccoli and Corn, and even some

Received: July 14, 2023
Revised: January 4, 2024
Accepted: January 11, 2024
Published: January 31, 2024

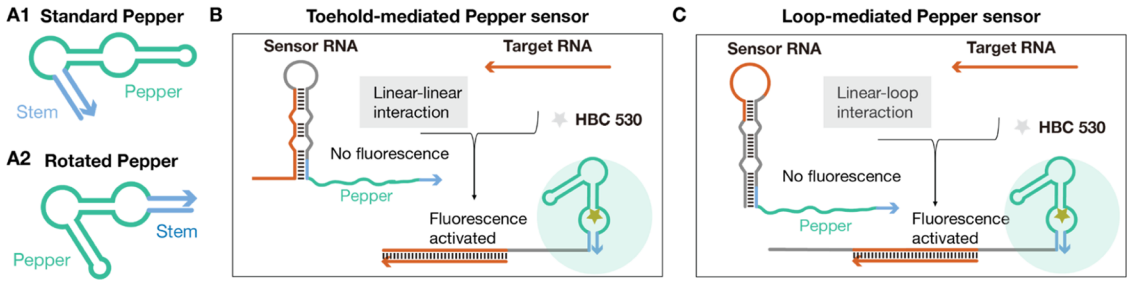

Figure 1. Overview of our Pepper RNA sensor design strategy and its variations. (A1) The secondary structure of the original Pepper aptamer. (A2) The secondary structure of the modified Pepper aptamer. (B) Schematic of the toehold-mediated Pepper sensor. (C) Schematic of the loop-mediated Pepper sensor.

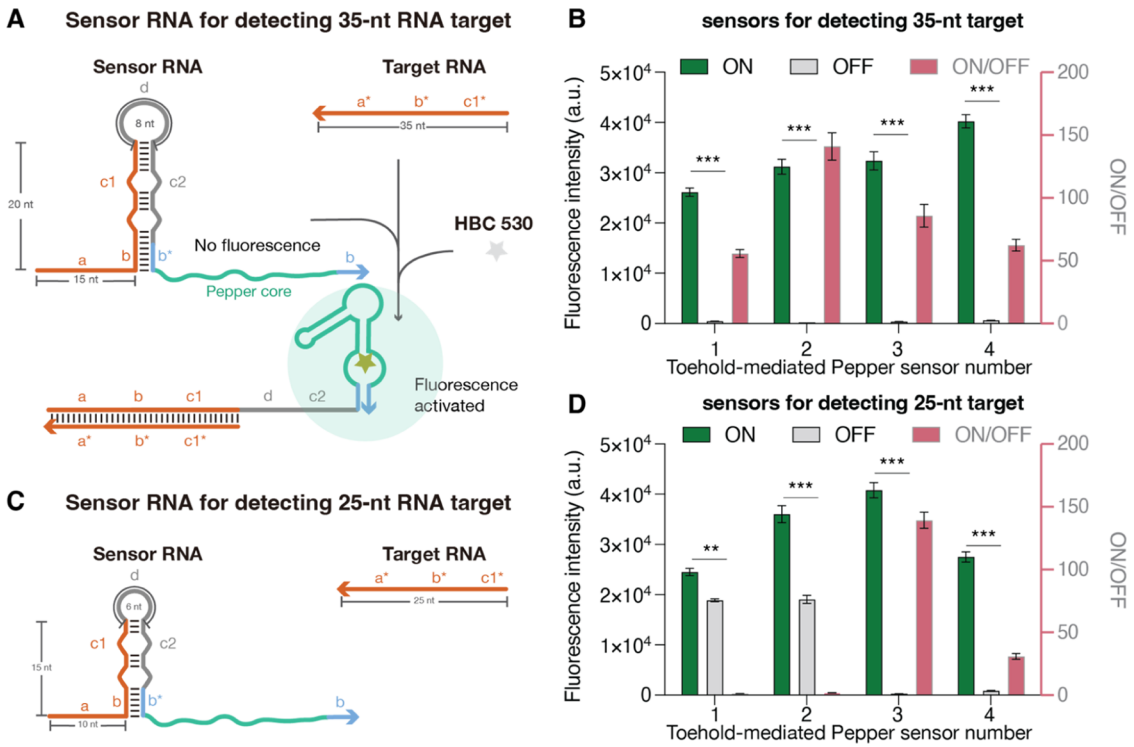

Figure 2. Toehold-mediated Pepper sensors. (A) Detailed schematic of the toehold-mediated Pepper sensor targeting 35-nucleotide target RNA. (B) Best-performing toehold-mediated Pepper sensors targeting arbitrary RNA targets. Data represent mean fluorescence intensity from plate reader measurements with sensor alone (OFF) and sensor plus 35-nucleotide target RNA (ON). ON/OFF ratios are shown in pink (right *y* axis). Error bars represent standard deviations from three technical replicates. (C) Schematic of the toehold-mediated Pepper sensor targeting 25-nucleotide target RNA. (D) Best-performing toehold-mediated Pepper sensors targeting shorter RNA targets. Data represent mean fluorescence intensity from plate reader measurements with sensor alone (OFF) and sensor plus 25-nucleotide target RNA (ON). Error bars represent standard deviations from three technical replicates. Significance: (***) for $p < 0.001$, (**) for $p < 0.01$.

fluorescent proteins such as mCherry.[10] Furthermore, in combination with various HBC analogs, Peppers can produce a diverse selection of bright and stable fluorescent complexes, offering a wide spectrum of emission maxima that extends from cyan to red.[10] An "inert Pepper" (iPepper) sensor was previously shown to detect endogenous RNA *in vivo* in different cell types.[27] In this system, the target RNA binds to and stabilizes the terminal ends of a misfolded Pepper aptamer, resulting in fluorescence activation. The system's optimization relied on a tandem array of iPepper (8×) and achieved an ON/OFF ratio of approximately 10-fold *in vitro*. To further improve the sensor ON/OFF ratio, alternative sensor design strategies are needed.

In this study, we introduce and demonstrate design approaches and generalizable optimization strategies for Pepper-based RNA sensors that can achieve up to 300-fold fluorescence enhancement *in vitro*. We demonstrate two types of Pepper sensor designs adapted from previous work demonstrating switchable RNA sensors[26,28−31] that take inspiration from RNA riboswitches developed for translation control in bacteria.[32,33] In both designs, the 5′ end of the Pepper stabilizing stem is sequestered in the stem-loop structure of the sensor, which destabilizes Pepper and forces it to adopt a nonfluorescent configuration (Figure 1B,C).[29] The first design, named the toehold-mediated sensor, employs a 5′ toehold domain to initiate the interaction with the target RNA strand and induce refolding of the aptamer into its fluorogenic conformation (Figure 1B). The second design, named the loop-mediated sensor, initiates the interaction with the target strand *via* the loop domain of its hairpin structure (Figure 1C). Using *in vitro* transcription and plate reader assays, we demonstrate that both sensors can be used to detect

https://doi.org/10.1021/acssynbio.3c00426
ACS Synth. Biol. 2024, 13, 498−508

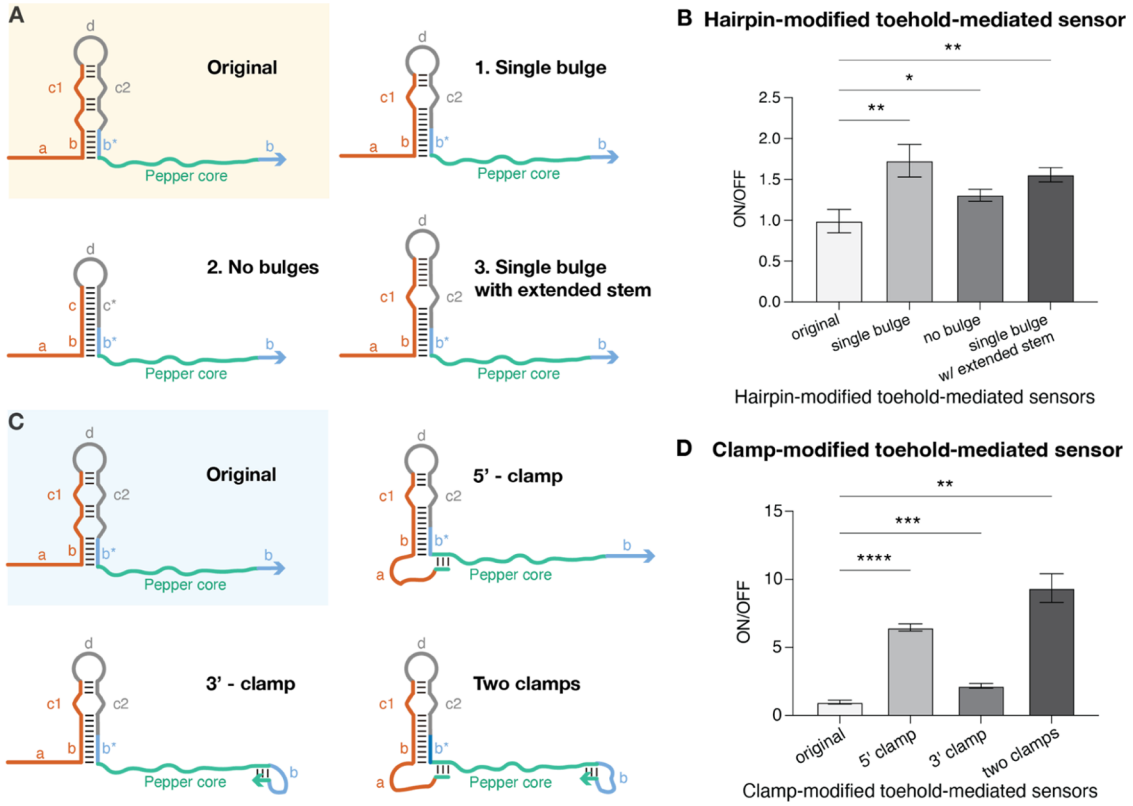

Figure 3. Forward-engineered toehold-mediated Pepper sensors. (A) Schematic of the design modifications made for the forward-engineered sensors. (B) Relative ON/OFF fluorescence ratio obtained for modified toehold-mediated Pepper sensors after 2 h of incubation. Error bars represent standard deviations from three technical replicates. (C) Schematic of the design modifications made for the sensors with single bulge. (D) Relative ON/OFF fluorescence ratio obtained for further modified toehold-mediated Pepper sensors after 2 h of incubation. Error bars represent standard deviations from three technical replicates. Significance: (****) for $p < 0.0001$, (***) for $p < 0.001$, (**) for $p < 0.01$, (*) for $p < 0.1$.

target RNA as short as 20 nt with no sequence constraints and a high dynamic range. Additionally, we offer strategies to enhance the performance of the sensor for a wide range of target RNA sequences. These strategies aim to reduce the sensor's leakage in the absence of the target RNA (sensor OFF) and to increase the fluorescence intensity of the sensor when the target RNA is present (sensor ON). Iterative application of these design strategies can result in a several hundred-fold increase in the ON/OFF ratio of a sensor. Using these design principles, we generate Pepper sensors for a range of specific, biologically relevant RNA sequences, including an MS2-repeat sequence, Tubulin α 1b (TUBA1B) transcript sequence, metastasis-associated lung adenocarcinoma transcript 1 (MALAT1) sequence, the A-repeat sequence of mouse and human X-inactive specific transcript (Xist/XIST) RNA, and the microRNA miR-302a, miR-294 and miR-124. Finally, we apply our optimization strategies to the Pepper sensor for detecting miR-294, achieving an ON/OFF ratio of approximately 300-fold.

Because our design, characterization, and optimization workflow is portable to any other type of FLAP, we expect our results will be immediately useful to build a variety of RNA sensors for the detection of biomarkers *in vitro*. The detection limits of our Pepper sensors have the potential to reach concentrations below those reported for the original target RNA within living cells. Furthermore, the efficacy of our RNA sensors was unaffected when tested in the presence of total RNA from HEK293 cells. The high sensitivity and remarkable robustness of the Pepper sensors underscore the feasibility of our design strategies for *in vivo* RNA sensing.

2. RESULTS AND DISCUSSION

2.1. Design of Toehold-Mediated Pepper Sensors.

The Pepper aptamer includes a fluorogen binding domain for its conjugate dye (HBC 530), which generates the fluorescent response, and a stem domain that stabilizes the aptamer structure (Figure 1A1). First, we wanted to test whether changes in the stem sequence affect the aptamer fluorescence, so we evaluated three Pepper aptamer variations with mutated stem sequences (Figure S1A), following the workflow in refs 27,29. In addition to the original Pepper aptamer, here referred to as standard Pepper (Figure 1A1), we considered circular permutations of Pepper, here referred to as rotated Pepper (Figure 1A2). We expected that the rotated Pepper, previously considered in ref 27, would have a higher tolerance to the stem sequence change because it has been shown that alterations at the terminal stem loop of the Pepper aptamer do not affect its fluorescence.[10] Our results showed that both standard and rotated Pepper had consistent fluorescence when their stem sequences were scrambled (Figure S1B). To begin with the sensor design, we first destabilized the Pepper aptamer and kept it in a nonfluorescent conformation by sequestering the 5′ end of the aptamer stem into a large hairpin structure. We then evaluated approaches to design the sensor and its target-binding region to achieve the release of the aptamer stem and refolding of the aptamer into its fluorescent conformation.

https://doi.org/10.1021/acssynbio.3c00426
ACS Synth. Biol. 2024, 13, 498−508

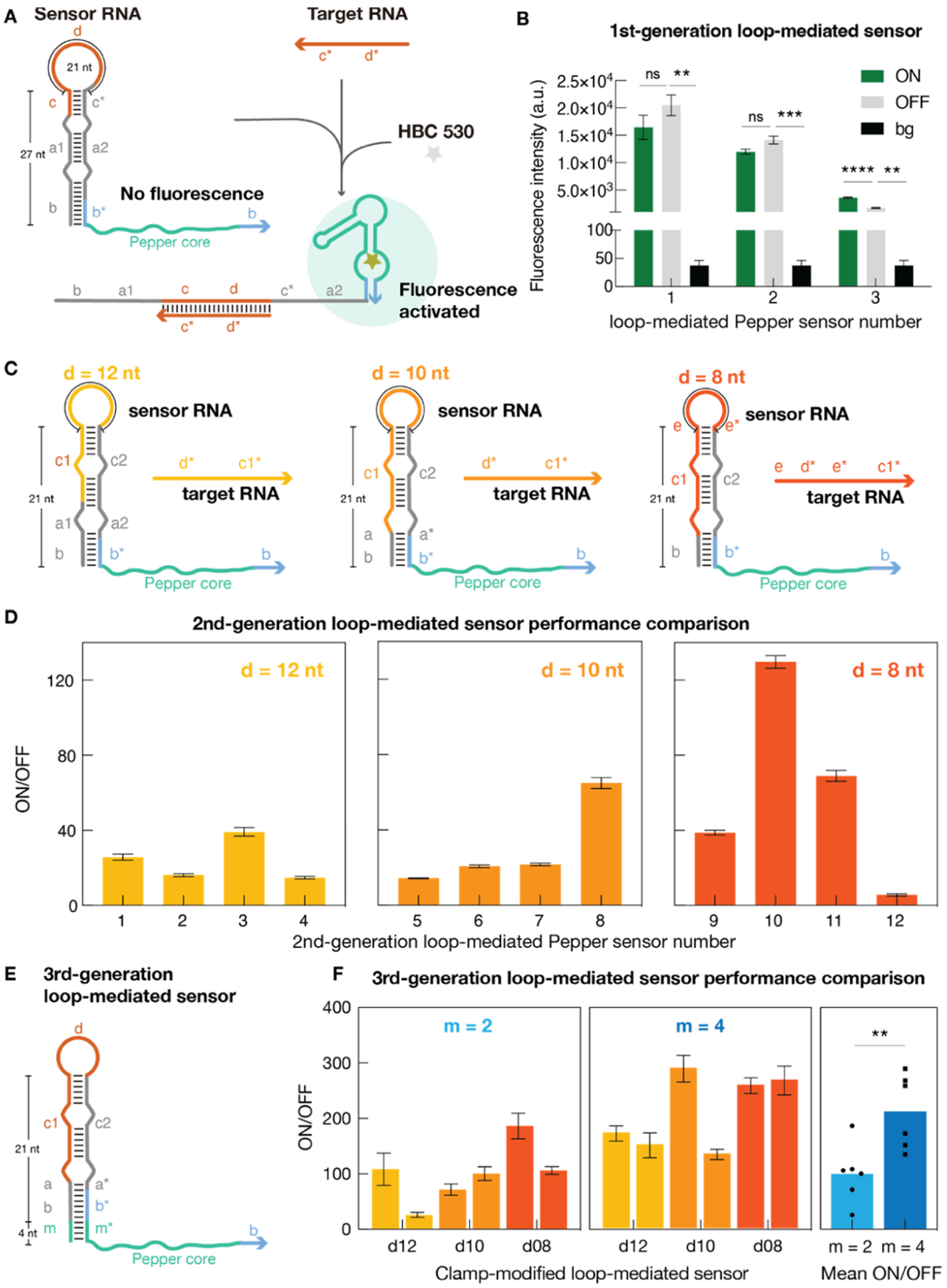

Figure 4. Development of loop-mediated Pepper sensors. (A) Detailed schematic of the loop-mediated Pepper sensor targeting 24-nucleotide target RNA. (B) Best-performing loop-mediated Pepper sensors targeting arbitrary RNA targets. Data represent mean fluorescence intensity from plate reader measurements with a sensor alone (OFF) and sensor plus 35-nucleotide target RNA (ON). Here, "bg" is the fluorescence signal from the HBC530 buffer in the absence of RNA. Error bars represent standard deviations from three technical replicates. (C) Schematic of the second-generation loop-mediated Pepper sensor targeting 24-nucleotide target RNA with various loop sizes. (D) Best-performing loop-mediated Pepper sensors targeting shorter RNA targets. Data represent mean fluorescence intensity from plate reader measurements with sensor alone (OFF) and sensor plus 24-nucleotide target RNA (ON). Error bars represent standard deviations from three technical replicates. (E). Schematic of the third-generation loop-mediated Pepper sensor that targets 24-nucleotide RNA. The size of the loop (**d** domain) is 12, 10, or 8 nt; the length of the clamp (**m** domain) is 4 or 2 nt. (F) Third-generation loop-mediated Pepper sensors and the mean ON/OFF comparison between two clamp designs. Data represent mean fluorescence intensity from plate reader measurements with sensor alone (OFF) and sensor plus 24-nucleotide target RNA (ON). Error bars represent standard deviations from three technical replicates. Significance: (****) for $p < 0.0001$, (**) for $p < 0.01$, (ns) for not significant.

https://doi.org/10.1021/acssynbio.3c00426
ACS Synth. Biol. 2024, 13, 498−508

The first design strategy (Figure 2A), named the toehold-mediated Pepper sensor, contains a 5′ toehold sequence as part of the target-binding region (orange), the core hairpin structure, and the Pepper aptamer sequence at the 3′ end (blue and green), following a strategy proposed in refs 28−30. The Pepper stem is initially sequestered with the **b*** domain of the core hairpin, thereby preventing binding of the fluorogen HBC 530 to the sensor RNA and resulting in a nonfluorescent (OFF) state in the absence of the target RNA. Upon the presence of target RNA, the toehold region of the sensor RNA initiates hybridization with the target, which mediates the strand-displacement reaction necessary for the conformational change of the sensor. This causes the unwinding of the core hairpin, thereby releasing the **b*** domain, which then hybridizes with the 3′ end of the **b** domain, leading to correct folding of the Pepper aptamer and resulting in high fluorescence (ON).

To start, we designed sensors to target arbitrary RNA sequences. This approach allowed us to assess the sensors under ideal conditions, where there were no sequence constraints at the toehold, loop (**d domain**), and **b domain**. The only fixed sequence was the Pepper core, highlighted in green. In other words, the target sequence was incorporated during the sequence optimization step. We generated toehold-mediated sensor candidates for detecting 35-nt RNA targets using the NUPACK nucleic acid sequence design package[17] and selected the top four sensor variants, with the least ensemble defects from the NUPACK prediction, for experimental testing using an *in vitro* plate reader assay (see Section 4). We found sensors adopting the rotated Pepper aptamer to be better performing, based on their low OFF signal and high ON signal when activated by their cognate target RNA (Figure 2B), when compared to the ones adopting the standard Pepper aptamer (Figure S1C). Therefore, we employed the rotated Pepper aptamer in subsequent sensor designs.

Next, we developed sensors that could detect shorter RNA targets: small noncoding RNAs, like small interfering RNA (siRNA) and microRNA (miRNA), are 19 to 25 nt in length and play important roles in gene regulation.[34] To make it possible to detect RNA targets of comparable length, we designed toehold-mediated sensors with a shorter sensing domain by changing (1) the length of the toehold region from 15 to 10 nt; (2) the length of the stem of the core hairpin from 20 to 15 nt; and (3) the size of the loop of the core hairpin from 8 to 6 nt (Figure 2C). We then generated and selected four toehold-mediated sensor variants with shorter sensing domain and evaluated them through our *in vitro* plate reader assay (Figures 2D and S1D). Among the four variants tested, sensors #3 and #4 exhibited better performance with negligible fluorescence leakage in their OFF state when compared with the background signal (Figures 2D and S1D). Our results suggest that the impact of sequence variation on sensor performance is greater in the sensor designed to detect 25-nt targets than in the sensor designed for 35-nt targets, possibly because of their shorter sensor domain.

2.2. Forward Engineering of the Toehold-Mediated Pepper Sensor. Next, we asked whether we could systematically engineer sensors to improve their ON/OFF ratio, and we focused on the variant with the worst performance (Figure 2D, toehold-mediated sensor no. 1 for detecting 25-nt RNA). We began by trying to minimize the signal leakage and made changes that include (1) removing the bottom bulge, (2) removing both bulges, and (3) removing the bottom bulge and extending the stem length (Figure 3A). The sensor with a single bulge showed the most notable improvements in its ON/OFF ratio (Figure 3B), and we kept this modification for our following designs.

We then re-examined the secondary structure predicted by NUPACK of all sensors we evaluated, and we noticed the structure-dependent factors that affect the performance of the sensors. The sensor leakage was decreased when the sequence at the two ends was predicted to interact with the rest of the sequence. We introduced these findings into the sensor design, as shown in Figure 3C, and we refer to these new modifications as clamps. A three-nucleotide sequence complementary to the Pepper core was added upstream of the sensing domain (orange) of the sensor for the 5′ clamp design, whereas a three-nucleotide sequence complementary to the Pepper core was added downstream of the **b** domain (blue) at the 3′ end of the sensor for the 3′ clamp design. When compared with the original sensor #1, the sensor with a single bulge and two clamps showed a significant increase of relative ON/OFF of 948% (Figure 3D). Our results suggest that the improvement in sensor performance achieved through the modification of the sensor stem and the addition of clamps to the sensor design was primarily due to the reduction in signal leakage (Figure S1E), rather than an enhancement in the brightness of the ON signal.

2.3. Design of Loop-Mediated Pepper Sensors. Although toehold-mediated Pepper sensors have a wide dynamic range and an ON/OFF ratio exceeding 100-fold (sensors #2 in Figure 2B and #3 in Figure 2D), their design has certain limitations regarding the stem sequence of Pepper (**b**/**b*** domain). In addition, these sensors require a long, single-stranded linear overhang, which is not well suited for RNA circularization techniques that are commonly used to enhance RNA stability and expression in mammalian cells.[35] To overcome these limitations, we developed an alternative design of the Pepper sensor that takes inspiration from loop-initiated RNA activators (LIRA)[33] and builds on earlier RNA sensors based on Broccoli aptamers.[29] By placing the target-binding region within the loop of the hairpin structure, the stem sequence of Pepper (**b**/**b*** domain) in the sensor becomes completely independent of the sequence of the cognate RNA target. Moreover, LIRAs have lower translational leakage compared to toehold-initiated riboregulators.[33] Therefore, if they could provide comparable ON signals to the toehold-mediated sensors, we anticipated that the loop-mediated sensors would exhibit a higher dynamic range.

Similar to the toehold-mediated sensor, the loop-mediated Pepper sensor includes a hairpin structure at the 5′ end to prevent folding of the downstream Pepper aptamer (Figure 4A). However, we began with a 27-nt-long hairpin stem and a 21-nt-long loop, adapting this "first-generation" sensor from the LIRA design. In this case, a 24-nt target RNA binds to exposed bases in the loop of the sensor RNA (orange domain), unwinding the hairpin stem and releasing the **b*** domain. The **b*** domain is expected to hybridize with the downstream **b** domain, facilitating the formation of the Pepper aptamer and the activation of the fluorescence. To evaluate this design idea, we generated loop-mediated sensor candidates using a NUPACK script and tested the three sensor-target variants with the lowest ensemble defects. At this stage, the target sequence was varied as part of the sequence optimization program.

https://doi.org/10.1021/acssynbio.3c00426
ACS Synth. Biol. 2024, 13, 498−508

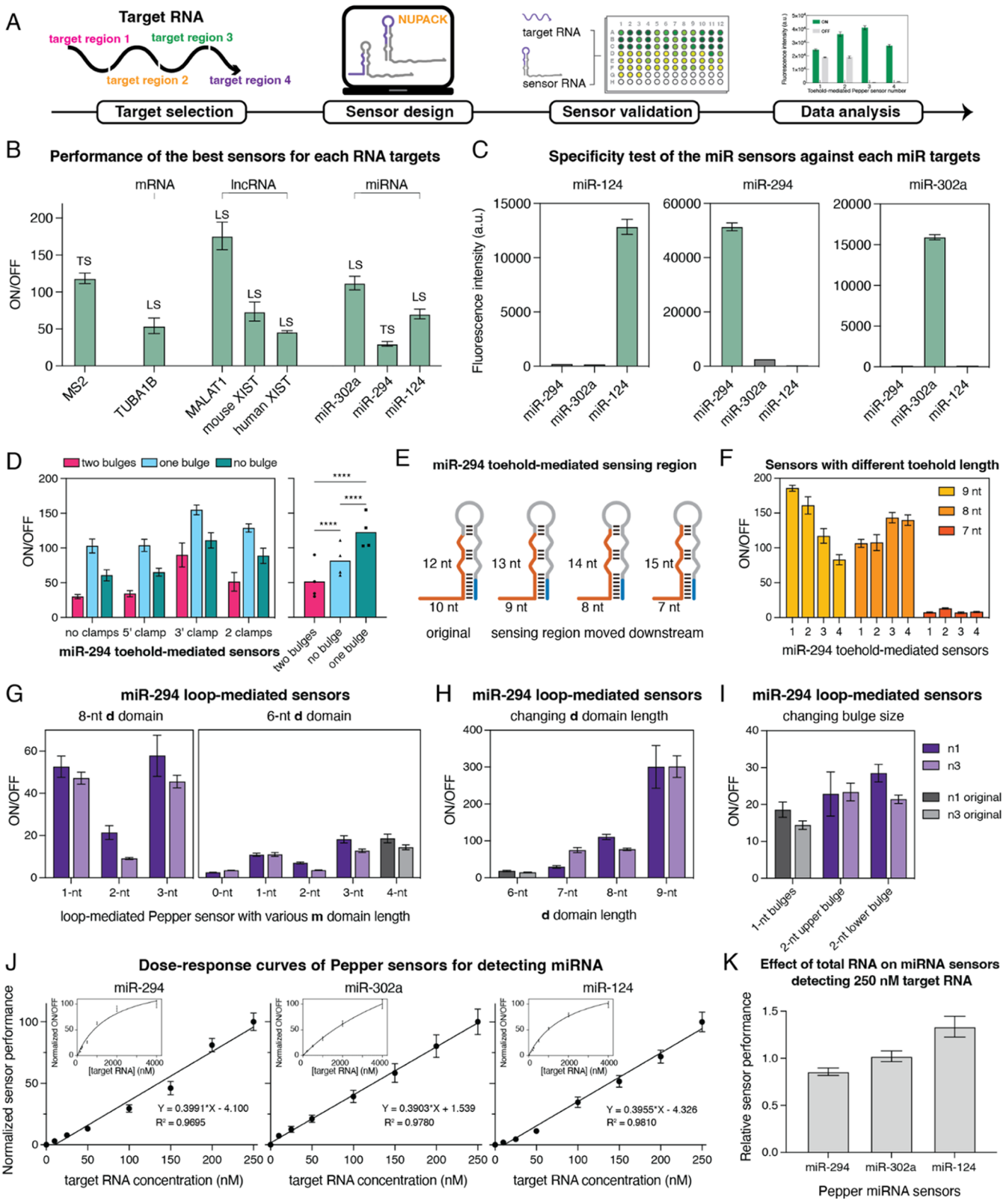

Figure 5. Optimization of Pepper sensors for detection of clinically relevant RNA targets. (A) Illustration of the workflow for developing a Pepper sensor for the detection of a sequence-specific RNA target. (B) ON/OFF ratios of the best-performing sensors for each synthetic RNA target. TS = toehold-mediated sensor; LS = loop-mediated sensor. (C) Specificity test for the three miR sensors measuring the fluorescence in the presence of each miR target. (D) The performance of the second-generation toehold-mediated sensors was designed for detecting miR-294. (E) Schematic of the modification of the third-generation toehold-mediated sensors for detecting miR-294. (F) ON/OFF ratios of the third-generation toehold-mediated sensors. (G) ON/OFF ratios of the loop-mediated sensors with various **m** domain lengths with 8- or 6-nt **d** domain. (H) The ON/OFF ratios of the loop-mediated sensors have **d** domains of 6, 7, 8, or 9 nt (4-nt **m** domain). (I) ON/OFF ratios of the loop-mediated sensors have a bulge size of 1 or 2 nt (4-nt **m** domain and 6-nt **d** domain). (J) Dose−response curves of the Pepper sensor detecting miRNA. The sensor

https://doi.org/10.1021/acssynbio.3c00426
ACS Synth. Biol. 2024, 13, 498−508

Figure 5. continued

performance (ON/OFF) exhibited a linear growth with increasing concentrations of miRNAs (0, 10, 25, 50, 100, 150, 200, and 250 nM miR-294, miR302a or miR124). Sensor performance data was normalized to the ON/OFF ratio observed in sensors with 250 nM target RNA to the sensor alone. Insets show the nonlinear regression of the normalized ON/OFF with a higher concentration of the target miRNA. LOD = $3.3\sigma/S$, where σ is the standard deviation of the regression and S is the slope of the calibration curve. (K) Relative ON/OFF of the sensors for detecting miRNA in total RNA extracts to the miRNA alone. Sensor RNA of 1 μM and target miRNA of 250 nM were used in the present and in the absence of 10× total RNA extracts. Measurements were taken 2 h after mixing in the plate reader. Error bars represent standard deviations from three technical replicates. Significance: (****) for $p < 0.0001$.

As shown in Figure 4B, each of the initial variants showed significant signal leakage in the absence of the target RNA, which in variants #1 and #2 surpassed the fluorescence in the ON state. To overcome this poor performance, we revised the sensor design parameters following steps similar to those taken for the toehold-mediated sensor, obtaining a "second-generation" set of sensors. For these sensors, while keeping the target sensing region length unchanged at 24 nt, we reduced the length of the hairpin (21 nt, two helical turns), making it comparable to the stem of the toehold-mediated Pepper sensor (Figure 4C). To generate a generalized design strategy for any given targets, we considered three loop sizes, 12, 10, and 8 nt, and for each size we generated and screened four sensor candidates with arbitrary target sequence (the target domain was not conserved, rather it was included in the NUPACK sequence optimization). Figure 4D shows that these adjustments immediately resulted in an increase in the ON/OFF ratio with a significant decrease in the OFF signal nearly 100-fold (Figure S1F). Our results suggested that our first-generation design of the 27-nt stem was not strong enough to hold a 21-nt loop in place and the fluorescent configuration is more favored.

We next hypothesized that the sensor performance could be further improved by limiting the spontaneous interaction of the **b*** domain with the downstream **b** domain, like in the toehold-mediated design. For this purpose, we built a series of third-generation sensors that include a clamp (**m**/**m*** domain) at the bottom of the hairpin (Figure 4E). We evaluated 2- or 4-nt-long **m**/**m*** domains that are complementary to the Pepper core sequence. For each case, we tested two candidate sensors against arbitrary target sequences (*i.e.*, the target sequence was optimized with the sensor domains). We observed greatly improved sensor performance compared to first- and second-generation loop-mediated sensors, with ultralow signal leakage detected (Figures 4F and S1F). On average (across arbitrary targets) the sensors with 4-nt clamps had higher ON/OFF ratios compared to the ones with 2-nt clamps.

2.4. Pepper Sensors for Detecting Sequence-Specific RNA Targets. Having confirmed that our design approach for Pepper sensors allows us to improve their ON/OFF ratio for arbitrary targets, we shifted our attention to building sensors for detecting specific biologically relevant RNA targets. We developed sensors to detect an MS2-repeat sequence and the mRNA of TUBA1b; long noncoding RNAs (lncRNAs) MALAT1 and mouse and human Xist/Xist RNA; and three microRNAs miR302-a, miR-294, and miR124. MS2-repeat sequences (consisting of 24 MS2 aptamer repeats) are widely used as a tag for live-cell mRNA imaging in conjunction with fluorescent protein labeled MS2 coat protein.[36,37] The TUBA1b mRNA was selected because of its ubiquitous importance across organisms: α/β-tubulin heterodimers are the basis of the dynamic cytoskeletal polymers—microtubules that are involved in various cellular functions.[38] MALAT1 is one of the best characterized lncRNAs, for its association with several types of human cancers.[39] Xist is another well-studied lncRNA that induces the transcriptional silencing of genes on one X chromosome in female cells.[40] We chose to detect the A-repeat sequence of the Xist RNA which recruits RNA-binding proteins necessary for the induction of X-linked gene silencing.[41] The Xist A-repeat region holds 7.5 and 8.5 copies of a conserved 26-nt sequence separated by U-rich linkers for human and mouse, respectively.[42] We targeted these conserved domains, and the specific sequence used for detection can be found in the Supporting Information (Pepper DNA template sequence). For each of these cases, we developed different Pepper RNA sensors (toehold- and loop-mediated) following the workflow outlined in previous sections (Figure 5A).

For long target RNAs, such as MS2-repeat, TUBA1B, and MALAT, we selected, respectively, four, two, and three target 20- or 24-nt subsequences from the full-length product. For shorter target RNAs, such as A-repeats of Xist RNA and the microRNAs, the targeting region is limited, so the target sequence is uniquely specified and identical to the full-length product. We validated and screened these sensors in the presence of 1x synthetic (*in vitro* transcribed) RNA targets, and Figure 5B shows the performance of the best sensors from a pool of three or four original toehold- and third-generation loop-mediated sensors for each RNA target sequence (the performance of the sensors is shown in Figures S2−S5, and sensor sequences can be found in the Supporting Information (SI) table). Six out of the eight sensors provide ON/OFF ratios over 50-fold upon detecting their specific target, and without any sensor optimization, the loop-mediated sensor for MALAT1 had an ON/OFF ratio of ∼176-fold. Moreover, the Pepper sensors for the microRNA showed very high specificity, as they can only be fully switched ON by their cognate RNA target when challenged with noncognate microRNA targets (Figure 5C).

We next tried to improve the best toehold-mediated Pepper sensor for miR-294, which showed the lowest ON/OFF ratio (30-fold) when compared to other sensors we tested (Figure 5B). We hypothesized that this is due to a combination of a high leakage signal in the absence of target and low on signal in the presence of target. We found high leakage to affect the ON/OFF ratio of all of the toehold-mediated sensors we tested against synthetic miR-294 targets (Figure S6). To reduce the leakage of the toehold-mediated sensors, we added clamps and reduced the number of bulges in the sensing stem of the sensor. We observed an improvement in performance with a smaller number of bulges and the addition of the 3′ clamp (Figure 5D). Further, we noticed that the **b** domain of the sensor contained three consecutive Gs and four Gs in total (5′GGGAAG), which explains why a 3′ clamp was effective. We then moved the sensing region down the sensor by 1 nt at a time (Figure 5E), so the three Gs were moved away from the bottom of the sensing stem. These newly designed sensors had

https://doi.org/10.1021/acssynbio.3c00426
ACS Synth. Biol. 2024, 13, 498−508

improved performance and exhibited reduced leakage only when the three Gs were flanked by other sequences within the **b** domain (sensors with 9- and 8-nt toehold) as shown in Figure 5F.

To enhance the signal intensity of the loop-mediated miR-294 sensors, we applied the design principles that we previously validated to the loop-mediated sensors N1 and N3: (1) shortening the length of the **m** domain from 4 nt to 3, 2, 1, or 0 nt; (2) increasing the length of the **d** domain from 6 to 7, 8, or 9 nt; and (3) changing the size of bulges within the sensing stem from 1 to 2 nt (Figure 5G−I). The sensors with the **m** domain removed had an ∼5-fold increase in ON signal for both N1 and N3, but they also had ∼37- and ∼20-fold increase in OFF state signal, respectively. Therefore, removing the **m** domain alone had an overall negative effect on the system. The sensors with a shortened **m** domain or an enlarged bulge had minimal effect on the brightness of the ON signal, whereas the sensors with a longer **d** domain had various degrees of signal enhancement. The best two sensors with 9-nt **d** domain modification displayed ON/OFF ratios of ∼300-fold. We also sought to improve the ON/OFF ratio of the Xist RNA sensors. The conserved sequences within the Xist A-repeat region created a nonlinear secondary structure preventing the binding of the target RNA. We applied similar sequence-based modifications to the sensor design (as we did for the miR-294 sensors), and the ON/OFF of the second-generation loop-mediated sensors for the mouse Xist A-repeats improved by ∼17-fold (Figure S7A−D). Our optimization strategies successfully improved the performance of both the Xist RNA sensors and the miR-294 sensors, demonstrating their potential applicability for various target-specific sensors.

2.5. Detection Range and Robustness of RNA Pepper Sensors. The capability of the sensors to detect the target RNA hinges on whether the target RNA concentration falls within the sensor's detection range. We determined the limit of detection (LOD) for our miRNA sensors by performing experiments that use a range of target miRNA concentrations from 0 to 250 nM (Figure 5J). The LOD was calculated to be 53.5, 45.2, and 42.0 nM for miR-294, miR-302a, and miR-124 sensors, respectively (LOD = $3.3\sigma/S$, where σ is the standard deviation of the regression and S is the slope of the calibration curve). The LOD values were found to be below the concentration of the abundantly expressed miRNA: miR-294 and miR-302a.[43,44] However, the LOD value was above the typical concentration of miR-124 reported in mESC.[45] It is important to note that for the LOD experiments, both sensor and target RNA underwent column purification and experienced freeze−thaw cycles and were not thermally annealed: this means that the folding of a significant fraction of the RNA molecules may differ from their cotranscriptional structure, which was used in the majority of our sensor-target selection experiments. We hypothesize that the sensitivity of the sensor could potentially improve when it attains cotranscriptional folding.

Another important aspect of sensor development is its robustness, which we define as its capacity to detect RNA targets in an environment containing a large number of RNA molecules that could introduce off-target effects. To evaluate the robustness of our Pepper sensor, we investigated its ability to differentiate specific target RNA within total RNA extracts from mammalian cells. We examined the performance of the miRNA sensor in the presence and absence of 10× the total RNA background, and we observed no discernible differences between the two scenarios (Figure 5K). Our results suggest the potential feasibility of employing the sensitive and robust Pepper sensors for *in vivo* miRNA detection.

3. CONCLUSIONS AND OUTLOOK

Here, we developed two types of Pepper-based fluorogenic RNA sensors that provide RNA detection capabilities *in vitro*. Both toehold- and loop-mediated Pepper sensors exhibit a wide dynamic range. We demonstrated the *in vitro* detection of RNA targets of lengths varying between 20 and 35 nt. We devised approaches to optimize toehold- and loop-mediated sensors' performances for arbitrary target RNA, building upon previous work that established such RNA sensors for diagnostic applications using other aptamers.[28−30] Our toehold-mediated sensor design originally included two 2-nt bulges in the hairpin structure to prevent premature transcription termination[46] and increase the thermodynamic stability of target−sensor interactions. However, our results suggest that the ON/OFF ratio of these sensors can be improved by approximately 10-fold through the removal of the bottom bulge in the hairpin structure and the incorporation of two clamps (Figure 3D). After two rounds of successive improvement, especially with the addition of the clamp at the bottom of the sensor stem, 10 out of 12 of the third-generation loop-mediated sensors we tested showed over 100-fold enhancement in fluorescence upon hybridizing with their cognate target RNA. Due to their low background fluorescence in the absence of target RNA, six of these sensors exhibit an ON/OFF ratio exceeding 150-fold. Furthermore, we developed Pepper sensors for detecting various mRNA, lncRNA, and microRNA targets with high specificity (Figure 5C). When considering the top-performing target-specific sensors presented in Figure 5B and the most effective miR-294 sensor from Figure 5H, the average ON/OFF ratio reached 119.1, with the highest ratio being 301 and the lowest at 46.

The Pepper sensor exhibits a signal-to-background ratio exceeding that of a superquenched DNA molecular beacon.[47] The highest-performing superquenched molecular beacon, utilizing FAM−3 DABCYLs, achieved a fluorescence signal enhancement of 320-fold through background fluorescence subtraction. Our second-generation loop-mediated Pepper sensors, utilizing a domain **d** of 9-nt, can achieve a fluorescence signal enhancement of approximately 550-fold through background fluorescence subtraction. Additionally, the Pepper sensor, being pure RNA-based, offers the advantage of reduced invasiveness due to its potential for endogenous expression, which distinguishes it from delivery methods such as microinjection and Microporation typically employed with molecular beacons.

In comparison to previously developed fluorescent light-up RNA-based sensors for detecting microRNA,[18,19,22,23] both of our optimized toehold-mediated and loop-mediated sensors demonstrated significantly greater ON/OFF ratios *in vitro*. Because these previously developed sensors have demonstrated utility in live-cell RNA localization or ratiometric imaging applications,[11,12,16,18,19,21,22,24−27] we anticipate that our Pepper sensors could be a valuable tool for RNA detection and tracking *in vivo*. To support this claim, we assessed the sensitivity of the Pepper sensors by conducting target RNA titration experiments using our highest-performing sensors. As shown in Figures 5J and S8, our results indicated that all seven of the selected sensors at 1 μM were activated by a target RNA concentration as low as 50 nM, which is below most of the

https://doi.org/10.1021/acssynbio.3c00426
ACS Synth. Biol. 2024, 13, 498−508

reported *in vivo* concentrations of target RNA in the literature.[43−45] Achieving this sensor/target RNA ratio is feasible when expressing the sensor in a medium or high copy number plasmid *in vivo*[48] Furthermore, we evaluated the robustness of the Pepper sensors in a complex RNA environment by spiking the target RNA into total RNA extracted from HEK 293 cells at various ratios [target]:[background]. We observed no significant change in sensor performance, and the sensors maintained their detection capabilities with up to 50-fold of the amount of total RNA (Figures S9 and 5K). Additional studies are needed to verify the specificity of the sensor for the detection of RNA; depending on the applications, discrimination of targets with small mutations may be desirable or preferable to detect a range of targets with a broad set of mutations. Although we did not develop Pepper sensors that are intentionally permissive of mismatches, we developed Pepper sensors for the consensus sequence of the Xist A-repeat. Our hope was that these sensors could tolerate sequence variants, thereby amplifying the signal, without the need for additional tandem sensing modules. Our results for sensors against the mouse Xist A-repeat variants indicated that the toehold-mediated sensor exhibits greater robustness to the presence of sequence mismatches when compared to the loop-mediated sensor (Figure S10). We conjecture that systematic sequence improvements could produce RNA sensors with the capacity to discern target mutations and respond exclusively to a particular mutant.

For expression in cells, our sensors will need to be modified to increase their stability, for example, by including a three-way junction motif or a tRNA motif that is known to enhance the stability of the ON-state aptamers.[49] To optimize sensors for *in vivo* RNA detection, we expect that our *in vitro* design/test/revision cycle will be useful to improve their signal-to-background ratio even when they include additional motifs. Although at the moment other sensors have greater sensitivity than the sensors we demonstrated here,[19] our rational design pipeline made it possible for us to build sensors that have a very high signal/background ratio *in vitro*, a parameter that is important in complex samples that could have a high level of background sensing. Our study lays groundwork for the advancement of RNA sensors that exhibit exceptional specificity and sensitivity toward diverse RNA targets. Furthermore, these sensors have the potential to be universally applicable across multiple organisms.

4. METHODS

4.1. Toehold- and Loop-Mediated Pepper Sensor Design. All our Pepper sensor variants were designed with NUPACK.[17] We report the scripts in the SI. The sensor strands with the lowest number of normalized ensemble defects were selected as candidates for *in vitro* experiments.

4.2. Sample Preparation. DNA templates for *in vitro* transcription were purchased from Integrated DNA Technologies. DNA oligonucleotides were amplified using Phusion High-Fidelity PCR Master Mix with HF Buffer (M0531L, New England BioLabs). AmpliScribe T7-Flash Transcription Kit (ASF3507, Lucigen) was used according to the manufacturer protocol with 4 μL of PCR products per 20 μL reaction. RNA was transcribed at 37 °C for 30 min, and the transcription was terminated with the addition of DNase I (Lucigen, ASF3507). Samples from this transcription mix were used directly without any purification in the plate reader screening experiments.

4.3. Plate Reader Sensor Screening. Sensors were screened in 96-well assay plates containing 2 μL of sensor RNA sample, 4 μL of target RNA sample, 2 μM HBC 530, 40 mM HEPES, 5 mM MgCl2, 100 mM KCl, and water for a final reaction volume of 100 μL. The fluorescence was monitored on a plate reader (BioTek H1) every minute for 2 h at 37 °C. For each sensor variant, the ON signal level was the fluorescence signal measured for the sensor in the presence of the target, whereas the OFF signal level was the fluorescence signal of the sensor alone, in the absence of target. To evaluate the performance of each sensor variant, we report the ON/OFF ratio throughout the paper. The ON and OFF signals were measured at 1 min intervals for 2 h, and the ON/OFF were calculated from data at 2 h time points, unless otherwise specified. Although a background control containing all buffer components was measured, it was not subtracted for the ON/OFF calculation. We conducted three replicates of the experiment.

4.4. RNA Extraction. Cell-extracted RNA was collected from Hek293 cells. Cells were maintained in media composed of 10% FBS (Life Technologies, 10099141), 100 mM L-glutamine (GIBCO, 25030−081), 1× MEM nonessential amino acids (NEAA) (GIBCO,11140−050), and 0.1 mM 2-mercaptoethanol (GIBCO, 21985−023) in DMEM (Sigma, D6429). The cells were harvested, washed with DPBS, and collected with Direct-zol (Zymo Research). RNA was extracted using the Direct-Zol RNA miniprep kit (Zymo Research) and quantified using a NanoDrop ND-1000 spectrophotometer (Thermo Scientific).

4.5. Limit of Detection Test and miRNA Detection in Total RNA. The sensor RNA and target RNA were transcribed as previously described. Subsequently, purification was carried out employing the Monarch RNA Cleanup Kit (T2040L, New England BioLabs). The concentration of both the sensor and target RNA was determined *via* a NanoDrop ND-1000 spectrophotometer (Thermo Scientific). Experimental samples were prepared in 96-well assay plates, comprising 1 μM sensor RNA, varying concentrations of target RNA, 2 μM HBC 530, 40 mM HEPES, 5 mM MgCl2, 100 mM KCl, and water to attain a final reaction volume of 100 μL. In the case of miRNA detection within total RNA samples, 250 nM target RNA and 2500 nM (10×) total RNA were employed, unless otherwise specified. The fluorescence was monitored on a plate reader (BioTek H1) every minute for 2 h at 37 °C. We reported the data from the 2 h time point.

■ ASSOCIATED CONTENT

Supporting Information

The Supporting Information is available free of charge at https://pubs.acs.org/doi/10.1021/acssynbio.3c00426.

DNA templates used in this study (XLSX)

Example Nupack script for designing Pepper sensor; Pepper variations and the Pepper sensor for arbitrary targets; performance of the sensors for detecting sequence-specific RNA targets; ON and OFF fluorescence signal for the first-generation miR-294 Pepper sensors; optimization of the Xist A-repeat sensors; Pepper sensor sensitivity for target-specific RNA sensors; effects of background RNA on example sensors; and overview of the performance of previously developed FLAP-based devices (PDF)

https://doi.org/10.1021/acssynbio.3c00426
ACS Synth. Biol. 2024, 13, 498−508

AUTHOR INFORMATION

Corresponding Author

Elisa Franco − *Department of Mechanical and Aerospace Engineering, University of California at Los Angeles, Los Angeles, California 90095, United States; Department of Bioengineering and Molecular Biology Institute, University of California at Los Angeles, Los Angeles, California 90095, United States;* orcid.org/0000-0003-1103-2668; Email: efranco@seas.ucla.edu

Authors

Anli A. Tang − *Department of Mechanical and Aerospace Engineering, University of California at Los Angeles, Los Angeles, California 90095, United States*

Anna Afasizheva − *Department of Biological Chemistry, David Geffen School of Medicine at the University of California Los Angeles, Los Angeles, California 90095, United States*

Clara T. Cano − *Department of Biological Chemistry, David Geffen School of Medicine at the University of California Los Angeles, Los Angeles, California 90095, United States*

Kathrin Plath − *Molecular Biology Institute, University of California at Los Angeles, Los Angeles, California 90095, United States; Department of Biological Chemistry, David Geffen School of Medicine at the University of California Los Angeles, Los Angeles, California 90095, United States; Jonsson Comprehensive Cancer Center, Brain Research Institute, Graduate Program in the Biosciences, Eli and Edythe Broad Center of Regenerative Medicine and Stem Cell Research, University of California Los Angeles, Los Angeles, California 90095, United States*

Douglas Black − *Molecular Biology Institute, University of California at Los Angeles, Los Angeles, California 90095, United States; Jonsson Comprehensive Cancer Center, Brain Research Institute, Graduate Program in the Biosciences, Eli and Edythe Broad Center of Regenerative Medicine and Stem Cell Research and Department of Microbiology, Immunology, and Molecular Genetics, University of California Los Angeles, Los Angeles, California 90095, United States*

Complete contact information is available at: https://pubs.acs.org/10.1021/acssynbio.3c00426

Author Contributions

E.F., K.P., and D.B. initiated and supervised the project. A.A.T. conducted the majority of experiments and data analysis. A.A. and C.T.C. participated in cell culture and RNA extraction. A.A.T. and E.F. wrote the manuscript. K.P. and D.B. contributed to manuscript editing. All of the authors have read and approved the final manuscript.

Notes

The authors declare no competing financial interest.

ACKNOWLEDGMENTS

E.F. acknowledges support from the UCLA Eli and Edythe Broad Center of Regenerative Medicine and Stem Cell Research Rose Hills Foundation Innovator Grant, from the HHMI Gilliam fellowship program, and from NSF award MCB 2020039. The authors thank Alexander Green and Ming Hammond for comments on the manuscript.

REFERENCES

(1) Babendure, J. R.; Adams, S. R.; Tsien, R. Y. Aptamers Switch on Fluorescence of Triphenylmethane Dyes. *J. Am. Chem. Soc.* **2003**, *125* (48), 14716−14717.

(2) Grate, D.; Wilson, C. Laser-Mediated, Site-Specific Inactivation of RNA Transcripts. *Proc. Natl. Acad. Sci. U.S.A.* **1999**, *96* (11), 6131−6136.

(3) Yerramilli, V. S.; Kim, K. H. Labeling RNAs in Live Cells Using Malachite Green Aptamer Scaffolds as Fluorescent Probes. *ACS Synth. Biol.* **2018**, *7* (3), 758−766.

(4) Filonov, G. S.; Moon, J. D.; Svensen, N.; Jaffrey, S. R. Broccoli: Rapid Selection of an RNA Mimic of Green Fluorescent Protein by Fluorescence-Based Selection and Directed Evolution. *J. Am. Chem. Soc.* **2014**, *136* (46), 16299−16308.

(5) Paige, J. S.; Wu, K. Y.; Jaffrey, S. R. RNA Mimics of Green Fluorescent Protein. *Science* **2011**, *333* (6042), 642−646.

(6) Strack, R. L.; Disney, M. D.; Jaffrey, S. R. A Superfolding Spinach2 Reveals the Dynamic Nature of Trinucleotide Repeat-Containing RNA. *Nat. Methods* **2013**, *10* (12), 1219−1224.

(7) Warner, K. D.; Sjekloća, L.; Song, W.; Filonov, G. S.; Jaffrey, S. R.; Ferré-D'Amaré, A. R. A Homodimer Interface without Base Pairs in an RNA Mimic of Red Fluorescent Protein. *Nat. Chem. Biol.* **2017**, *13* (11), 1195−1201.

(8) Dolgosheina, E. V.; Jeng, S. C. Y.; Panchapakesan, S. S. S.; Cojocaru, R.; Chen, P. S. K.; Wilson, P. D.; Hawkins, N.; Wiggins, P. A.; Unrau, P. J. RNA Mango Aptamer-Fluorophore: A Bright, High-Affinity Complex for RNA Labeling and Tracking. *ACS Chem. Biol.* **2014**, *9* (10), 2412−2420.

(9) Autour, A.; Jeng, S. C. Y.; Cawte, A. D.; Abdolahzadeh, A.; Galli, A.; Panchapakesan, S. S. S.; Rueda, D.; Ryckelynck, M.; Unrau, P. J. Fluorogenic RNA Mango Aptamers for Imaging Small Non-Coding RNAs in Mammalian Cells. *Nat. Commun.* **2018**, *9* (1), No. 656, DOI: 10.1038/s41467-018-02993-8.

(10) Chen, X.; Zhang, D.; Su, N.; Bao, B.; Xie, X.; Zuo, F.; Yang, L.; Wang, H.; Jiang, L.; Lin, Q.; Fang, M.; Li, N.; Hua, X.; Chen, Z.; Bao, C.; Xu, J.; Du, W.; Zhang, L.; Zhao, Y.; Zhu, L.; Loscalzo, J.; Yang, Y. Visualizing RNA Dynamics in Live Cells with Bright and Stable Fluorescent RNAs. *Nat. Biotechnol.* **2019**, *37* (11), 1287−1293.

(11) Alam, K. K.; Tawiah, K. D.; Lichte, M. F.; Porciani, D.; Burke, D. H. A Fluorescent Split Aptamer for Visualizing RNA-RNA Assembly In Vivo. *ACS Synth. Biol.* **2017**, *6* (9), 1710−1721.

(12) Wang, Z.; Luo, Y.; Xie, X.; Hu, X.; Song, H.; Zhao, Y.; Shi, J.; Wang, L.; Glinsky, G.; Chen, N.; Lal, R.; Fan, C. In Situ Spatial Complementation of Aptamer-Mediated Recognition Enables Live-Cell Imaging of Native RNA Transcripts in Real Time. *Angew. Chem., Int. Ed.* **2018**, *57* (4), 972−976.

(13) Yu, Q.; Ren, K.; You, M. Genetically Encoded RNA Nanodevices for Cellular Imaging and Regulation. *Nanoscale* **2021**, *13* (17), 7988−8003.

(14) Kolpashchikov, D. M. Binary Malachite Green Aptamer for Fluorescent Detection of Nucleic Acids. *J. Am. Chem. Soc.* **2005**, *127* (36), 12442−12443.

(15) Kikuchi, N.; Kolpashchikov, D. M. A Universal Split Spinach Aptamer (USSA) for Nucleic Acid Analysis and DNA Computation. *Chem. Commun.* **2017**, *53* (36), 4977−4980.

(16) Mudiyanselage, A. P. K. K. K.; Yu, Q.; Leon-Duque, M. A.; Zhao, B.; Wu, R.; You, M. Genetically Encoded Catalytic Hairpin Assembly for Sensitive RNA Imaging in Live Cells. *J. Am. Chem. Soc.* **2018**, *140* (28), 8739−8745, DOI: 10.1021/jacs.8b03956.

(17) Zadeh, J. N.; Steenberg, C. D.; Bois, J. S.; Wolfe, B. R.; Pierce, M. B.; Khan, A. R.; Dirks, R. M.; Pierce, N. A. NUPACK: Analysis and Design of Nucleic Acid Systems. *J. Comput. Chem.* **2011**, *32* (1), 170−173.

(18) Huang, K.; Doyle, F.; Wurz, Z. E.; Tenenbaum, S. A.; Hammond, R. K.; Caplan, J. L.; Meyers, B. C. FASTmiR: An RNA-Based Sensor for in Vitro Quantification and Live-Cell Localization of Small RNAs. *Nucleic Acids Res.* **2017**, *45* (14), No. e130.

(19) Ying, Z.-M.; Wu, Z.; Tu, B.; Tan, W.; Jiang, J.-H. Genetically Encoded Fluorescent RNA Sensor for Ratiometric Imaging of

MicroRNA in Living Tumor Cells. *J. Am. Chem. Soc.* **2017**, *139* (29), 9779−9782.
(20) Bhadra, S.; Ellington, A. D. A Spinach Molecular Beacon Triggered by Strand Displacement. *RNA* **2014**, *20* (8), 1183−1194.
(21) Kitto, R. Z.; Christiansen, K. E.; Hammond, M. C. RNA-Based Fluorescent Biosensors for Live Cell Detection of Bacterial sRNA. *Biopolymers* **2021**, *112* (1), No. e23394.
(22) Dou, C.-X.; Liu, C.; Ying, Z.-M.; Dong, W.; Wang, F.; Jiang, J.-H. Genetically Encoded Dual-Color Light-Up RNA Sensor Enabled Ratiometric Imaging of MicroRNA. *Anal. Chem.* **2021**, *93* (4), 2534−2540.
(23) Aw, S. S.; Tang, M. X.; Teo, Y. N.; Cohen, S. M. A Conformation-Induced Fluorescence Method for microRNA Detection. *Nucleic Acids Res.* **2016**, *44* (10), No. e92.
(24) Ong, W. Q.; Citron, Y. R.; Sekine, S.; Huang, B. Live Cell Imaging of Endogenous mRNA Using RNA-Based Fluorescence "Turn-On" Probe. *ACS Chem. Biol.* **2017**, *12* (1), 200−205.
(25) Sato, S.-I.; Watanabe, M.; Katsuda, Y.; Murata, A.; Wang, D. O.; Uesugi, M. Live-Cell Imaging of Endogenous mRNAs with a Small Molecule. *Angew. Chem., Int. Ed.* **2015**, *54* (6), 1855−1858.
(26) Wang, T.; Simmel, F. C. Switchable Fluorescent Light-up Aptamers Based on Riboswitch Architectures. *Angew. Chem., Int. Ed.* **2023**, *62*, No. e202302858, DOI: 10.1002/anie.202302858.
(27) Wang, Q.; Xiao, F.; Su, H.; Liu, H.; Xu, J.; Tang, H.; Qin, S.; Fang, Z.; Lu, Z.; Wu, J.; Weng, X.; Zhou, X. Inert Pepper Aptamer-Mediated Endogenous mRNA Recognition and Imaging in Living Cells. *Nucleic Acids Res.* **2022**, *50* (14), No. e84.
(28) Yan, Z.; Tang, A. A.; Eshed, A.; Ticktin, Z. M.; Chaudhary, S.; Ma, D.; McCutcheon, G.; Li, Y.; Wu, K.; Saha, S.; Alcantar-Fernandez, J.; Moreno-Camacho, J. L.; Campos-Romero, A.; Collins, J. J.; Yin, P.; Green, A. A.Rapid and Multiplexed Nucleic Acid Detection Using Programmable Aptamer-Based RNA Switches *medRxiv* 2023 DOI: 10.1101/2023.06.02.23290873.
(29) Tang, A. RNA Aptamer-Based Systems for Pathogen Detection and Biomolecule Synthesis; Doctoral thesis Arizona State University, 2020.
(30) Green, A.; Ma, D.; Tang, A. Unimolecular Aptamer-Based Sensors for Pathogen Detection. U.S. Patent US20, 2017.
(31) Green, A. Molecular Fuses for Real-Time, Label-Free, Multiplexed Imaging of RNAs in Living Cells. US11,047,000, 2021.
(32) Green, A. A.; Silver, P. A.; Collins, J. J.; Yin, P. Toehold Switches: De-Novo-Designed Regulators of Gene Expression. *Cell* **2014**, *159* (4), 925−939.
(33) Ma, D.; Li, Y.; Wu, K.; Yan, Z.; Tang, A. A.; Chaudhary, S.; Ticktin, Z. M.; Alcantar-Fernandez, J.; Moreno-Camacho, J. L.; Campos-Romero, A.; Green, A. A. Multi-Arm RNA Junctions Encoding Molecular Logic Unconstrained by Input Sequence for Versatile Cell-Free Diagnostics. *Nat. Biomed. Eng.* **2022**, *6* (3), 298−309.
(34) Lam, J. K. W.; Chow, M. Y. T.; Zhang, Y.; Leung, S. W. S. siRNA Versus miRNA as Therapeutics for Gene Silencing. *Mol. Ther. Nucleic Acids* **2015**, *4* (9), No. e252.
(35) Litke, J. L.; Jaffrey, S. R. Highly Efficient Expression of Circular RNA Aptamers in Cells Using Autocatalytic Transcripts. *Nat. Biotechnol.* **2019**, *37* (6), 667−675.
(36) Markaki, Y.; Chong, J. G.; Wang, Y.; Jacobson, E. C.; Luong, C.; Tan, S. Y. X.; Jachowicz, J. W.; Strehle, M.; Maestrini, D.; Banerjee, A. K.; Mistry, B. A.; Dror, I.; Dossin, F.; Schöneberg, J.; Heard, E.; Guttman, M.; Chou, T.; Plath, K. Xist Nucleates Local Protein Gradients to Propagate Silencing across the X Chromosome. *Cell* **2021**, *184* (25), No. 6212, DOI: 10.1016/j.cell.2021.11.028.
(37) Wu, B.; Chao, J. A.; Singer, R. H. Fluorescence Fluctuation Spectroscopy Enables Quantitative Imaging of Single mRNAs in Living Cells. *Biophys. J.* **2012**, *102* (12), 2936−2944.
(38) Kim, N. D.; Park, E.-S.; Kim, Y. H.; Moon, S. K.; Lee, S. S.; Ahn, S. K.; Yu, D.-Y.; No, K. T.; Kim, K.-H. Structure-Based Virtual Screening of Novel Tubulin Inhibitors and Their Characterization as Anti-Mitotic Agents. *Bioorg. Med. Chem.* **2010**, *18* (19), 7092−7100.
(39) Amodio, N.; Raimondi, L.; Juli, G.; Stamato, M. A.; Caracciolo, D.; Tagliaferri, P.; Tassone, P. MALAT1: A Druggable Long Non-Coding RNA for Targeted Anti-Cancer Approaches. *J. Hematol. Oncol.* **2018**, *11* (1), No. 63, DOI: 10.1186/s13045-018-0606-4.
(40) Loda, A.; Heard, E. Xist RNA in Action: Past, Present, and Future. *PLoS Genet.* **2019**, *15* (9), No. e1008333.
(41) Colognori, D.; Sunwoo, H.; Wang, D.; Wang, C.-Y.; Lee, J. T. Xist Repeats A and B Account for Two Distinct Phases of X Inactivation Establishment. *Dev. Cell* **2020**, *54* (1), 21−32.e5.
(42) Pintacuda, G.; Young, A. N.; Cerase, A. Function by Structure: Spotlights on Xist Long Non-Coding RNA. *Front. Mol. Biosci.* **2017**, *4*, No. 90.
(43) Bosson, A. D.; Zamudio, J. R.; Sharp, P. A. Endogenous miRNA and Target Concentrations Determine Susceptibility to Potential ceRNA Competition. *Mol. Cell* **2014**, *56* (3), 347−359.
(44) Morin, R. D.; O'Connor, M. D.; Griffith, M.; Kuchenbauer, F.; Delaney, A.; Prabhu, A.-L.; Zhao, Y.; McDonald, H.; Zeng, T.; Hirst, M.; Eaves, C. J.; Marra, M. A. Application of Massively Parallel Sequencing to microRNA Profiling and Discovery in Human Embryonic Stem Cells. *Genome Res.* **2008**, *18* (4), 610−621.
(45) Yeom, K.-H.; Mitchell, S.; Linares, A. J.; Zheng, S.; Lin, C.-H.; Wang, X.-J.; Hoffmann, A.; Black, D. L. Polypyrimidine Tract-Binding Protein Blocks miRNA-124 Biogenesis to Enforce Its Neuronal-Specific Expression in the Mouse. *Proc. Natl. Acad. Sci. U.S.A.* **2018**, *115* (47), E11061−E11070.
(46) Lesnik, E. A.; Sampath, R.; Levene, H. B.; Henderson, T. J.; McNeil, J. A.; Ecker, D. J. Prediction of Rho-Independent Transcriptional Terminators in *Escherichia Coli*. *Nucleic Acids Res.* **2001**, *29* (17), 3583−3594.
(47) Yang, C. J.; Lin, H.; Tan, W. Molecular Assembly of Superquenchers in Signaling Molecular Interactions. *J. Am. Chem. Soc.* **2005**, *127* (37), 12772−12773.
(48) Phillips, G. J.; Park, S. K.; Huber, D. High Copy Number Plasmids Compatible with Commonly Used Cloning Vectors. *Biotechniques* **2000**, *28* (3), 400−408.
(49) Filonov, G. S.; Kam, C. W.; Song, W.; Jaffrey, S. R. In-Gel Imaging of RNA Processing Using Broccoli Reveals Optimal Aptamer Expression Strategies. *Chem. Biol.* **2015**, *22* (5), 649−660.